PERGAMON

Scripta mater. 44 (2001) 1139–1146

Scripta MATERIALIA

www.elsevier.com/locate/scriptamat

CHARACTERIZATION BY INDENTATION OF COMBUSTION SYNTHESIZED CERMETS

Eugene A. Olevsky[1], Elizabeth R. Strutt[2] and Marc A. Meyers[2]

[1]Department of Mechanical Engineering, San Diego State University, 5500 Campanile Dr., San Diego, CA 92182-1323 [2]Department of Mechanical and Aerospace Engineering, University of California, San Diego, 9500 Gilman Dr., La Jolla, CA 92093-0404

(Received January 2, 2000)
(Accepted in revised form September 4, 2000)

Abstract—Results of indentation experiments used for the determination of the deformation response of the combustion synthesized TiC-NiTi composite are described. The experimentally obtained data is used in combination with a model developed for the indentation process which enables the calculation of the constitutive properties of a porous cermet.

Keywords: Cermet; Self-propagating high-temperature synthesis; Indentation

1. Introduction

Uniaxial pressing with a pressure-transmitting medium (*i.e.* PTM) (Fig. 1) has been attracting attention [1].

Known as the Ceracon [2] or Quasi-Isostatic Pressing (*i.e.* QIP) process, it has been utilized industrially in manufacturing [3] and more recently, in combination with self-propagating high-temperature synthesis (*i.e.* SHS) [4–9]. Highly exothermic reactions that become self-sustaining and propagate as a combustion wave provide an attractive low cost alternative for the production of refractory ceramics and composites.

Unlike conventional sintering, which requires heating for long times at high temperatures, combustion synthesis uses an external energy source only for local ignition, and the reaction is complete within seconds. It has been shown that when this technique is combined with external pressure, dense products can be formed from reactant powders. One of the appropriate processing techniques used for the external pressure application is the above-mentioned Quasi-Isostatic-Pressing. When combined with SHS, QIP offers a relatively simple processing method by which hundreds of industrially-useful materials can be produced and shaped into engineering components. A granular pressure-transmitting medium (alumina with graphite powder) not only serves as a load transmitter, but also as a natural thermal insulator which prevents substantial heat loss and minimizes temperature gradients during SHS.

For this study, TiC-NiTi composites were made by combustion synthesis and densification in a granular pressure transmitting medium. TiC-NiTi composites allow for optimization of material properties by combining the hard, wear resistant properties of ceramics with the increased ductility of the metal phases.

In light of the current development of near-net-shape technologies, the analysis of both shape and volume changes under QIP is of considerable importance.

The factors which influence the shape and volume change of a porous body include the initial porosities of both the PTM and porous body, and their respective constitutive properties. The investi-

PII: S1359-6462(01)00661-3

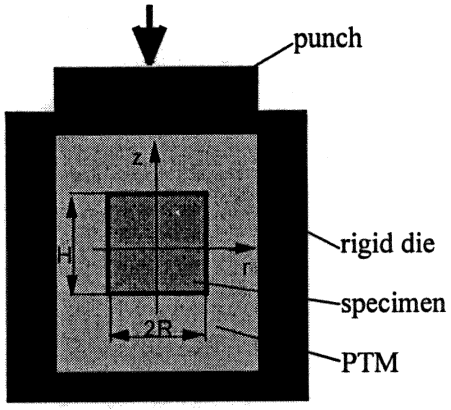

Figure 1. Loading mode under quasi-isostatic pressing.

gation of the effect of these factors on shape change during QIP is one of the objectives of the earlier work [10]. To apply the developed model for the description of shape change of a porous specimen produced from specific material, the constitutive properties of the porous body skeleton should be known. The present work includes the results of the indentation experiments used for the determination of the deformation response of the combustion synthesized TiC-NiTi composite. The experimentally obtained data is used in combination with a developed model of the indentation process which enables the calculation of the rheological parameters of a porous cermet.

2. Experimental Procedure and Results of Indentation

The starting materials used in this investigation were high purity powders of Ti, C, and Ni. The Ti powder (99.7% pure) from Micron Metals was classified as -325 mesh with the smallest dimension being less than 44 μm. The C powder (99.9% pure) from Consolidated Astronautics had a particle size of 2 μm with a flake-like morphology. It tended to form large agglomerates on the order 50 μm. The Ni powder (99.7% pure) from Aldrich Chemical Co had an average particle size of 3 μm with a filament structure.

Powder was mixed in order to obtain final product compositions corresponding to volume fraction of NiTi of 0.3. The combustion temperature for this composition is about 2600°K [11]. Since sintered TiC-NiTi composites [12,13] typically have a lattice parameter of 4.32×10^{-4} μm,which corresponds to $TiC_{0.7}$, samples were also prepared anticipating nonstoichiometric carbide.

The powders were loaded under argon into polyethylene jars and dry mixed with burundum™ grinding media (4:1 by weight) for at least 24 hours. Then they were baked in a vacuum oven for a minimum of 24 hours at approximately 100°C and a pressure less than 100 mm Hg to remove adsorbed water. After baking, the powders were uniaxially pressed in a steel die into a green compact having diameter of 80 mm and height of 15 mm. The relative density of the cold pressed compact was 0.5.

The green compact was placed on a 2mm layer of an alumina refractory sheet as a thermal insulator (see Fig. 2) to protect it from immediate cooling after combustion synthesis. The indentation experiment was carried out using a screw driven testing machine with the controlled variable velocity of the punch (indentor) movement.

The velocity of the indentor movement was 0.41 mm/s. The indentor was a SiC rod with diameter of 15 mm. The sample was ignited remotely with a variable transformer. The time delay between the end of the combustion and the beginning of the indentation was 10s.

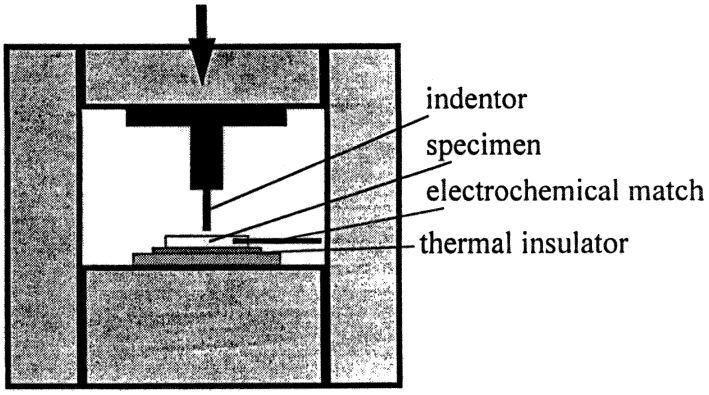

Figure 2. Indentation schematics.

A reconstructed image of the indented specimen is represented in Fig. 3. The material domain located below the indentor was densified to about 100% relative density, while the peripheral layers underwent swelling during combustion synthesis and had an increased final porosity (of about 60%).

The mechanical response of the cermet material is represented in Fig. 4 in the form of the stress-engineering strain (axial deformation of the material domain below the indentor) dependence. The material hardening during indentation should be attributed to the decrease of porosity, cooling of the material during indentation and possible physical hardening of the porous body skeleton.

3. Modeling the Indentation of the Combustion Synthesized Porous Cermet

The mechanical properties of the porous cermet immediately after combustion synthesis can be identified as nonlinear-viscous (power-law creep). Mechanical response of a nonlinear-viscous porous body can be described [14–16] by a constitutive relationship connecting components of stressss tensor σ_{ij} and strain rate tensor $\dot{e}_{ij}$:

$$\sigma_{ij} = A\left(\frac{\sqrt{\varphi\dot{\gamma}^2 + \psi\dot{e}^2}}{\sqrt{1-\theta}}\right)^{n-1}\left[\varphi\dot{e}_{ij} + \left(\psi - \frac{1}{3}\psi\right)\dot{e}\delta_{ij}\right] \tag{1}$$

where A and n- are material creep parameters; φ and ψ are the shear and bulk normalized viscosity moduli, which depend on porosity φ (for example, following [16], $\varphi = (1-\theta)^2$, $\psi = \frac{2(1-\theta)^3}{3\theta}$; δ_{ij}, is a Kronecker symbol (δ_{ij}, if i = j, and δ_{ij}, if i ≠ j); $\dot{e}$ is the first invariant of the strain rate tensor, *i.e.* sum of tensor diagonal components: $\dot{e} = \dot{e}_{11} + \dot{e}_{22} + \dot{e}_{33}$.

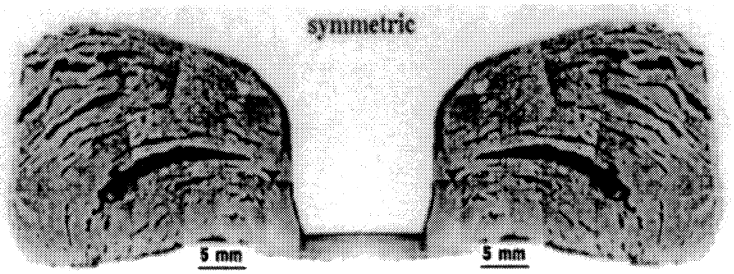

Figure 3. Reconstructed image of the indented TiC-TiNi composite.

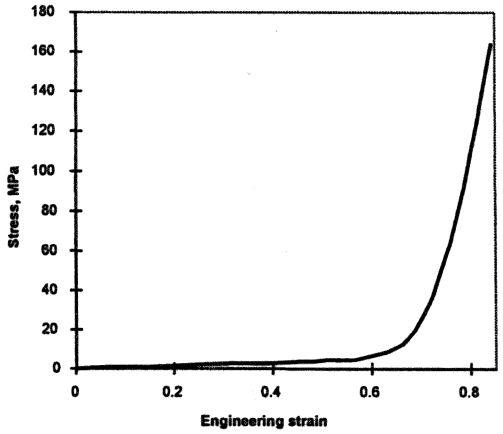

Figure 4. The mechanical response of the cermet material during indentation.

Equivalent strain rate W is connected with the current porosity and with the invariants of the strain rate tensor:

$$W = \frac{1}{\sqrt{1-\theta}}\sqrt{\varphi\dot{\gamma}^2 + \psi\dot{e}^2} \tag{1}$$

Term $\dot{\gamma}$ is the second invariant of the strain rate tensor deviator and represents, physically, the shape change rate of a porous body:

$$\dot{\gamma} = \left[\left(\dot{e}_{ij} - \frac{1}{3}\dot{e}\delta_{ij}\right)\left(\dot{e}_{ij} - \frac{1}{3}\dot{e}\delta_{ij}\right)\right]^{1/2} \tag{2}$$

It can be noted, that, for n = 1, Equation (1) is transformed into a relationship describing a linear-viscous constitutive response ($A = 2\eta_0$, where η_o is the shear viscosity of the porous body skeleton) and, for n = 0, Equation (1) is transformed into a relationship corresponding to rigid-plastic properties of the porous body skeleton ($A = \tau_0$, where τ_o is the yield stress of the porous body skeleton). Thus, linear-viscous and rigid-plastic behavior are two limiting cases for nonlinear-viscous constitutive properties.

With regard to expressions for φ and ψ, the given model can be used for $\theta < \frac{2}{3}$.

3.1. Analytical Modeling of the Indentation Process

To get an analytical solution, the boundary conditions and the indentation load schematics should be simplified. In this connection, we shall consider the indentation as a uniaxial up-setting of a porous cylinder with a radius smaller that the radius of the indentor. Friction is neglected.

The volume-change rate $\dot{e}$ and the shape-change rate $\dot{\gamma}$ are given by:

$$\dot{e} = \dot{e}_{zz} 2\dot{e}_{rr} = \left[1 + 2\left(\frac{\dot{e}_{rr}}{\dot{e}_{zz}}\right)\right]\dot{e}_{zz} = \frac{\dot{\theta}}{1-\theta} \tag{3}$$

$$\dot{\gamma} = \sqrt{\frac{2}{3}}\left|\dot{e}_{zz} - \dot{e}_{rr}\right| = \sqrt{\frac{2}{3}}\left|1 - \left(\frac{\dot{e}_{rr}}{\dot{e}_{zz}}\right)\right|\left|\dot{e}_{zz}\right| \tag{4}$$

where $\dot{e}_{zz}$, $\dot{e}_{rr}$, and θ are the axial strain rate, radial strain rate, respectively. For a cylindrical specimen, the axial and radial strain rates are given by:

$$\dot{e}_{zz} = \frac{\dot{H}}{H}; \quad \dot{e}_{rr} = \frac{\dot{R}}{R} \tag{5}$$

where H and R are the instantaneous cylinder height and radius. Substituting Equation (6) into Equation (5) gives the following relationship for the shape-change rate:

$$\dot{\gamma} = \sqrt{\frac{2}{3}}\left|\frac{\dot{H}}{H} - \frac{\dot{R}}{R}\right| \tag{6}$$

This expression will be used to derive relationships between the height and radius of the cylindrical specimen and porosity.

The radial σ_{rr} and the axial σ_{zz} stresses can be written as (see Eq. (1)):

$$\sigma_{rr} = AW^{n-1}\varphi\left\{\left(\frac{\dot{e}_{rr}}{\dot{e}_{zz}}\right) - \frac{1}{3}\left[1 - 3\left(\frac{\psi}{\varphi}\right)\right]\left[1 + 2\left(\frac{\dot{e}_{rr}}{\dot{e}_{zz}}\right)\right]\dot{e}_{zz}\right\} \tag{7}$$

$$\sigma_{rr} = AW^{n-1}\varphi\left\{1 - \frac{1}{3}\left[1 - 3\left(\frac{\psi}{\varphi}\right)\right]\left[1 + 2\left(\frac{\dot{e}_{rr}}{\dot{e}_{zz}}\right)\right]\dot{e}_{zz}\right\} \tag{8}$$

The equivalent strain rate W is defined as (see (Eq.(2))

$$W = \left\{\frac{\varphi}{1-\theta}\left[\dot{\gamma}^2 + \frac{\psi}{\varphi}\dot{e}^2\right]\right\}^{\frac{1}{2}} = \left[(1-\varphi)\left\{\frac{2}{3}\left(1 - \frac{\dot{e}_{rr}}{\dot{e}_{zz}}\right)^2 + \frac{\psi}{\varphi}\left(1 + 2\left(\frac{\dot{e}_{rr}}{\dot{e}_{zz}}\right)\right)^2\right\}\right]^{\frac{1}{2}}|\dot{e}_{zz}| \tag{9}$$

During free up-setting, the applied stresses on the lateral surfaces are equal to zero (*i.e.* $\sigma_{rr} = 0$). From Equation (8) one can obtain the following relationship between the axial and radial strain rates:

$$\frac{\dot{e}_{rr}}{\dot{e}_{zz}} = \frac{1 - 3\left(\frac{\psi}{\varphi}\right)}{1 + 6\left(\frac{\psi}{\varphi}\right)} = \varphi\frac{2 - 3\theta}{4 - 3\theta} \tag{10}$$

Substituting Equation (11) into Equation (10) gives the following expression for the equivalent strain rate:

$$W = (6)^{\frac{1}{2}}\left[\frac{(1-\theta)}{(4-3\theta)^{\frac{1}{2}}}\right]|\dot{e}_{zz}|^n \tag{11}$$

Combining Equations (9), (11), and (12) and considering that $\sigma_{zz} < 0$, the following expression for the axial stress is obtained:

$$\sigma_{zz} = -A(6)^{\frac{n+1}{2}}\left[\frac{(1-\theta)^{n+2}}{(4-3\theta)^{\frac{n+1}{2}}}\right]|\dot{e}_{zz}|^n \tag{12}$$

The latter equation can be transformed as follows

$$\frac{|\sigma_z|}{A}\left(\frac{H_o}{V_p}\right)^n = 6^{\frac{n+1}{2}}\left[\frac{(1-\theta^{n+2}}{(4-3\theta)^{\frac{n+1}{2}}}\right]\left(\frac{H_o}{H}\right)^n \tag{13}$$

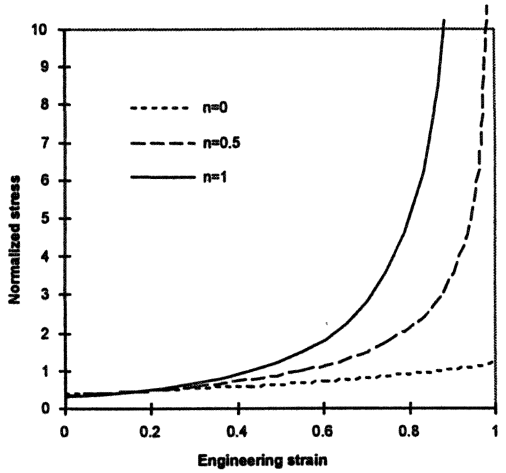

Figure 5. Analytical solution for the indentation approximated as an up-setting of a porous cylinder.

where H_o is the initial height of the porous cylinder, V_p is a constant velocity of the indentor. From Eqs. (4), (6), and (11) it follows that

$$\frac{\dot{\theta}}{1-\theta} = \frac{3\theta}{4-3\theta}\frac{\dot{H}}{H} \tag{14}$$

Integration of Eq. (15) gives

$$\left(\frac{\theta}{\theta_o}\right)^4 \frac{1-\theta_o}{1-\theta} = \left(\frac{H}{H_o}\right)^3 \tag{15}$$

where θ_o is the initial porosity before the indentation.

The solution of set of Eqs. (14) and (16) enables the determination of the stress-strain dependence characterizing the mechanical response of the porous material.

The dependence of the normalized stress $\dfrac{|\sigma_z|}{A\left(\dfrac{H_o}{V_p}\right)^n}$ on the engineering strain is shown in Fig. 5 for different values of the strain rate sensitivity n.

The engineering strain is calculated as $\dfrac{H_o - H}{H_o}$. Here it should be noted that the dimensionless normalized stress depends on the strain rate sensitivity n itself.

Using Eqs. (14) and (16), one can find the constitutive properties (coefficients A and n) which would provide the best fit for the experimental data given in Fig. 4. It is determined that the following values: $A = 180 MPa \cdot s^{0.2}$, $n = 0.2$ provide the best fit to the experimental data.

3.2. Finite-Element Modeling of the Indentation Process

The results of the analytical modeling can be accepted only as a rough assessment of the real mechanical behavior of the combustion synthesized material. In order to obtain more exact data, one needs to consider the corresponding boundary-value problem of the indentation. The finite-element algorithm, used for this purpose and based on the continuum theory of sintering [14–17], is described elsewhere [16]. The boundary conditions are reduced to the full bonding of the bottom surface. The friction is

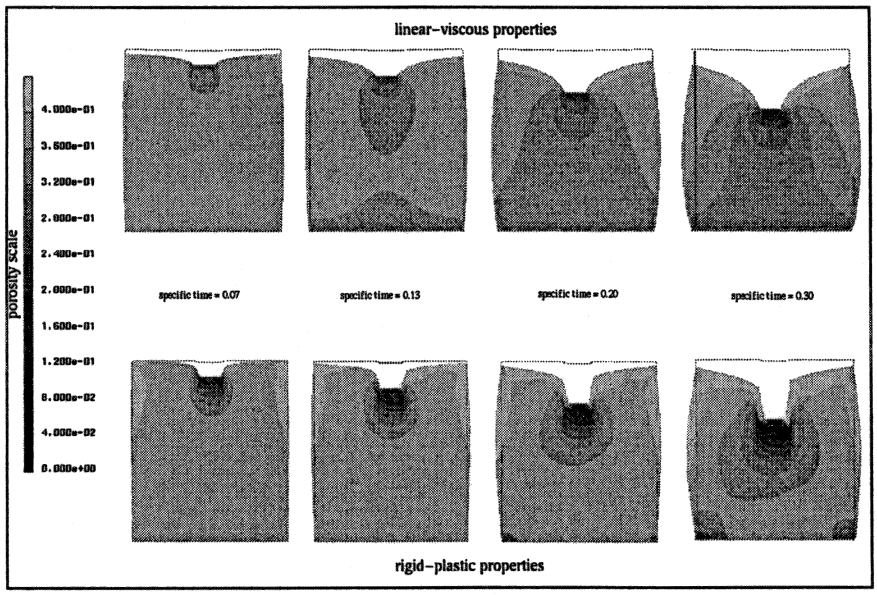

Figure 6. Results of the finite-element calculations of the indentation of a linear-viscous (n = 1) and rigid-plastic material (n = 0).

neglected. The initial porosity is assumed to be 40%. The constitutive behavior of the porous material is determined by relationship (1). The calculations results are represented in Fig. 6 for two limiting cases: n = 1 (linear-viscous material) and n = 0 (rigid-plastic material). The specific time used in the calculations is defined as 1/(30s)·t, where t is the physical time (s).

In Fig. 6, one can see more localized densification in the case of the rigid-plastic material.

The stress-strain relationship obtained from the calculations (the stress is counted as an integral of the reaction force over the indentor cross-section area) can be used for the solution of the inverse problem: to find the constitutive properties (coefficients A and n) which would provide the best fit for the experimental data given in Fig. 4. As a result of a number of "computer experiments," the best fitting values for A and n are found to be A = 100 MPa·$s^{0.18}$, n = 0.18. One can see (Fig. 7) that these values correspond to a lower deformation response of the porous material compared to the values obtained by analytical modeling. This is understandable, because the analytical model does not take into account the additional radial resistance of the peripheral layers, rendering the overestimated values of the material resistance. Fig. 7 provides also a comparison with the experimentally measured porosity of the compressed area below the indentor.

The porosity distribution as well as the final macroscopic shape of the indented specimen can be used as additional fitting parameters which is a subject of further investigations.

Conclusions

1. An experimental-theoretical integrated approach is developed for the determination of the constitutive properties of the combustion synthesized material.
2. A mathematical model of the hot indentation of the porous material is elaborated.
3. The constitutive (power-law creep) properties of the combustion synthesized TiC-TiNi composite are determined.

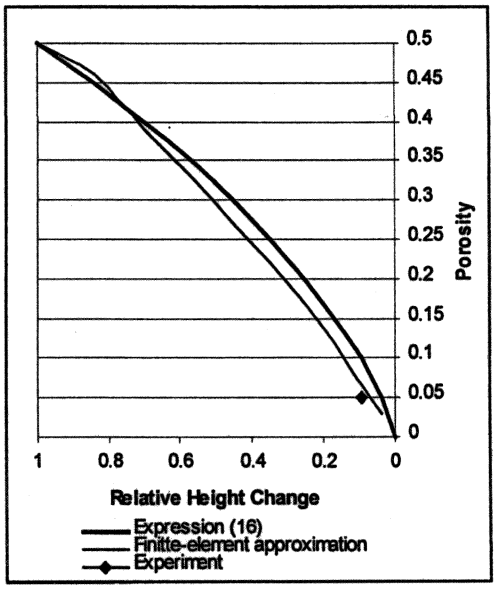

Figure 7. Comparison of porosity relative height dependence for experiment and finite element and analytical approximations.

Acknowledgments

This work has been in part supported by the NSF Division of Manufacturing and Industrial Innovation, Grant DMII–9985472. The technical assistance of J. Ma is appreciated.

References

1. R. M. German, Powder Metallurgy Science, 2nd edn., MPIF, Princeton NJ (1994).
2. R. V. Raman, S. V. Rele, S. Poland, J. LaSalvia, M. A. Meyers, and A. R. Niller, J. Met. 3, 23 (1995).
3. M. Ohyanagi, M. Fukushima, and M. Koizumi, in Proceedings of the International Conference on Hot Isostatic Pressing, Andover MA, pp. 289–294 (1996).
4. P. H. Shingu, K. N. Ishihara, F. Ghonome, T. Hyakawa, M. Abe, and K. Tagushi, in Proceedings of the 1st US-Japan Workshop on Combustion Synthesis (Tsukuba), pp. 65–71 (1990).
5. Y. V. Bogatov, E. Levashov, and A. N. Pityulin, Sov. Powder Metall. 7(343), 76 (1991).
6. B. Mihelic, M. Dikic, R. Djekic, and D. Uskokovic, Mater. Lett. 13, 391 (1992).
7. J. C. LaSalvia and M. A. Meyers, Int. J. SHS. 4, 43 (1995).
8. J. C. LaSalvia, D. K. Kim, R. A. Lipsett, and M. A. Meyers, Metall. Mater. Trans. A. 26A, 3001 (1995).
9. J. C. LaSalvia and M. A. Meyers, Metall. Mater. Trans. A. 26A, 3011 (1995).
10. E. A. Olevsky, E. R. Kristofetz, and M. A. Meyers, Int. J. SHS. 7(4), 517 (1998).
11. E. Olevsky, E. Kristofetz, C. Uzoigwe, and M. Meyers, Adv. Powder Met. Part. Mater. 3.43–3.49 (1997).
12. T. M. Poletika, S. N. Kul'kov, and V. E. Panin, Sov. Powder Metall. 7(247), 549 (1983).
13. S. N. Kul'kov, T. M. Poletika, A. Yu. Chukhlomin, and V. E. Panin, Sov. Powder Metall. 8(260), 88 (1984).
14. E. Olevsky, H. J. Dudek, and W. A. Kaysser, Acta Metall. Mater. 44, 707 (1996).
15. E. Olevsky, H. J. Dudek, and W. A. Kaysser, Acta Metall. Mater. 44, 715 (1996).
16. E. A. Olevsky, Mater. Sci. Eng. R. Rev. 23, 41 (1998).
17. E. A. Olevsky and R. M. German, Acta Mater. 48, 1153 (2000).
18. V. V. Skorohod, Rheological Basis of Theory of Sintering, Kiev, Naukova Dumka (1972).